PERGAMON

INTERNATIONAL JOURNAL OF
Plasticity

Micromechanical finite element calculations of temperature and void configuration effects on void growth and coalescence

M.F. Horstemeyer *, M.M. Matalanis, A.M. Sieber, M.L. Botos

Center for Materials and Engineering Sciences, MS9405, Sandia National Laboratories, Livermore, CA 94551-0969, USA

Abstract

We present micromechanical finite element results that quantify coalescence effects based upon temperature and different spatial arrangements of voids. We propose a critical intervoid ligament distance (ILD) to define void coalescence that is derived from micromechanical simulations in which void volume fraction evolves as a function of strain. Several parameters were varied using the temperature and strain rate internal variable plasticity model of Bammann–Chiesa–Johnson to determine the coalescence effects. The parameters include two types of materials with different work hardening rates (304L stainless steel and 6061T6 aluminum), three different temperatures (298, 400, and 600 K), several boundary conditions (force and displacement: uniaxial, plane strain, and biaxial), type of element used (plane strain and axisymmetric), different ILDs, and the number of voids (one and two void configurations). The present study provides a basis for macroscale modeling of coalescence which is briefly discussed. © 2000 Elsevier Science Ltd. All rights reserved.

Keywords: Constitutive behavior; Finite elements; Void coalescence; Elastic–viscoplastic material; Voids and inclusions

1. Introduction

Void nucleation, growth, and coalescence often characterize damage progression in ductile metals. Of the three components, the least amount of research has been

---

* Corresponding author. Fax: +1-510-294-3410.

E-mail address: mfhorst@sandia.gov (M.F. Horstemeyer).

performed on understanding void coalescence, which is typically associated with the last step of the idealized three stage damage process. Void coalescence realistically occurs at different spatial size scales throughout the deformation and is not just limited to final failure. Understanding coalescence throughout deformation is key for macroscale prediction of failure in finite element codes. As such, numerical and physical micromechanical studies can provide important information for constructing phenomenological equations that are necessary at higher spatial size scales. The purpose of this study is to provide such a database.

Within the last 20 years, different aspects of void coalescence have been examined. Garrison and Moody (1987) provide a thorough review of studies before 1987. Since that time, some work has focused on quantifying void coalescence. Faleskog and Shih (1997) recently performed planar micromechanical calculations based upon the constitutive model and numerical implementation of Cuitino and Ortiz (1992) and Moran et al. (1990). In the Faleskog and Shih (1997) study, different initial void volume fractions and different stress triaxialities were examined. Tvergaard and Needleman (1995, 1997) and Ramaswamy and Aravas (1998) have discussed void coalescence from a macroscale continuum perspective using an intrinsic spatial size scale parameter. Pardoen et al. (1998) compared four different coalescence criteria in finite element simulations and compared these results to experimental data for copper. Nagaki et al. (1993) examined void growth by coalescence from using different nearest neighbor distances in a numerical setting. Benson (1993) has numerically analyzed different void configurations (coalescence) for high strain rate shock environments. Eftis et al. (1991) examined void growth under high rate spall conditions and quantified void growth influences on the final damage state. Chan (1988) has analyzed void growth under high temperature creep environments. Recent physical experiments from studies in the materials science literature reveal a strong influence of coalescence on final failure of metals (cf. Jun, 1991; Worswick et al., 1994; Worswick and Pick, 1995; Geltmacher et al., 1996; 1998; Zurek et al., 1997; Tonks et al., 1997; Al-Ostaz and Jasiuk, 1997; Bandstra et al., 1998; Lu et al., 1998).

Coalescence of voids has typically been categorized into either void impingement or void sheeting. During void impingement, the material ligament between two voids necks to a point as the two neighboring voids grow together (Cottrell, 1959). The void sheet mechanism occurs by the following process. Primary voids can nucleate from second phase particles, and these voids grow as the material is plastically deformed. At a higher strain/stress level, neighboring particles will nucleate secondary voids. These particles tend to be smaller and have stronger bonds with the matrix. Then, voids from the larger particle distributions will link to the smaller void distribution through the ligament over a small interval of strain. The material path between the void distributions looks sheet-like, hence, the name "void sheet" mechanism.

In this study, we do not presuppose any mechanism for coalescence but simply start with spherical holes in a ductile matrix. Horstemeyer and Ramaswamy (2000) recently have examined various parameters in the context of void growth enhancement from coalescence, in which temperature dependence was shown to be qualitatively more important than void spacing, void distribution, void shape, and void

size. In this writing, we quantify the temperature effects by varying several parameters related to coalescence in a micromechanical setting using the temperature and strain rate internal variable plasticity model of Bammann, Chiesa and Johnson (BCJ) (1993, 1996):

1. number of voids (one void and various two void configurations),
2. three different temperatures (298, 400, and 600 K),
3. type of element used (planar 2D and axisymmetric),
4. intervoid ligament distance (ILD),
5. boundary conditions (force and displacement: uniaxial, plane strain, and biaxial), and
6. materials with different work hardening rates (304L stainless steel and 6061T6 aluminum).

2. Micromechanics analysis

In this section, we describe the finite element framework and assumptions and then discuss the BCJ plasticity model. We note that the term micromechanics has the connotation of "micron" scale, but these calculations are performed in the context of the locality postulate of mechanics and thus are size scale invariant.

2.1. Finite element preliminaries

The ABAQUS-Standard finite element program (Hibbitt et al., 1998) was used to solve the large strain, void growth problems in this study. By using finite element analysis, we determined the void configuration and temperature effects upon void growth and coalescence. Quarter space analyses were used with one void and half space analyses were used with two voids. Nodal constraints were placed on the free boundaries to ensure that a plane remained a plane during the simulations. The various void configurations are shown in Fig. 1. Most of the two void calculations included an ILD of one void diameter to ensure coalescence. However, we also performed calculations varying the ILD to determine a critical ILD that defines the point of coalescence.

To avoid confusion about plane strain boundary conditions and plane strain elements used in our calculations, we use the term "planar 2D" when referring to the plane strain *element* calculations and "plane strain" when referring to the boundary conditions. Hence, when a plane strain boundary condition was imposed upon a planar 2D calculation, the nodes in the x direction were fixed, so the strain in the x direction was zero from the fixed nodes and the strain in the z direction was zero from the type of element used. For a plane strain boundary condition with an axisymmetric element, the radial strain is fixed to zero from the boundary condition and the strain in the theta direction is zero from the type of element used.

When the element type was changed from a planar 2D to an axisymmetric element, the initial void volume fraction was slightly different. When comparing these

two simulation results, we plot the normalized void volume fraction (void volume fraction divided by the initial void volume fraction, which is the same as the void volume divided by the initial void volume) as a function of von Mises strain.

The term configuration is used in the context of this study was the orientation of two voids with the loading direction. Three types of void configurations for the planar 2D calculations and two for the axisymmetric calculations were used. For the planar 2D calculations, we created meshes for one void, two voids collinear with the *y*-axis, and two voids collinear with the *x*-axis. For the axisymmetric calculations, we created meshes for one void and two voids collinear with the *y*-axis. We did not use the two void configuration in which the voids were collinear with the *x*-axis because the outer void would be annular instead of spherical. One might suggest that fully three dimensional simulations are warranted to accurately model void growth; however, Thomson et al. (1998) showed that one void axisymmetric simulations gave almost identical results as three dimensional simulations.

2.2. Temperature and strain rate plasticity model

ABAQUS-standard was used with the thermodynamically based BCJ internal variable constitutive equations. The equations used within the context of the finite
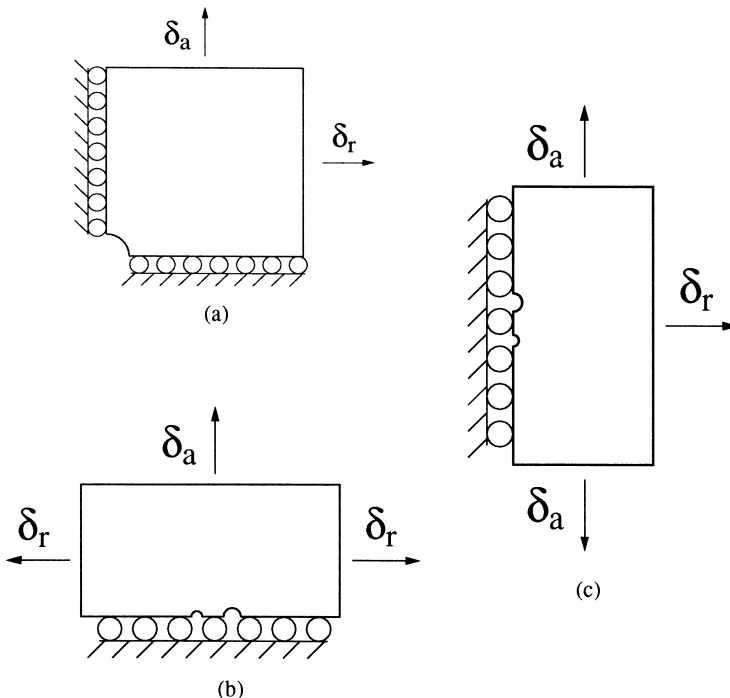

Fig. 1. Geometry configurations of voids and boundary conditions for the (a) one void, (b) two void-orientation 2, and (c) two void-orientation 1.

element method are the rate of change of the observable and internal state variables given by,

$$\overset{\circ}{\underline{\sigma}} = \underline{\dot{\sigma}} - \underline{W}^e\underline{\sigma} - \underline{\sigma}\,\underline{W}^e = \lambda(1-D)\text{tr}(\underline{D}^e)\underline{I} + 2\mu(1-D)\underline{D}^e - \frac{\dot{D}}{1-D}\underline{\sigma} \tag{1}$$

$$\underline{D}^e = \underline{D} - \underline{D}^{\text{in}}. \tag{2}$$

$$\underline{D}^{\text{in}} = f(T)\sinh\left[\frac{\left\|\underline{\sigma}' - \underline{\alpha}\right\| - \{R + Y(T)\}\{-D\}}{V(T)\{1-D\}}\right]\frac{\underline{\sigma}' - \underline{\alpha}}{\left\|\underline{\sigma}' - \underline{\alpha}\right\|}, \tag{3}$$

$$\overset{\circ}{\underline{\alpha}} = \underline{\dot{\alpha}} - \underline{W}^e\underline{\alpha} + \underline{\alpha}\,\underline{W}^e = h(T)\underline{D}^{\text{in}} - \left[\sqrt{\frac{2}{3}}r_{\text{d}}(T)\left\|\underline{D}^{\text{in}}\right\| + r_{\text{s}}(T)\right]\left\|\underline{\alpha}\right\|\underline{\alpha}, \tag{4}$$

$$\dot{R} = H(T)\underline{D}^{\text{in}} - \left[\sqrt{\frac{2}{3}}R_{\text{d}}(T)\left\|\underline{D}^{\text{in}}\right\| + R_{\text{s}}(T)\right]R^2, \tag{5}$$

and are generally written as objective rates ($\overset{\circ}{\underline{\sigma}}$, $\overset{\circ}{\underline{\alpha}}$) with indifference to the continuum frame of reference assuming a Jaumann rate in which the continuum spin equals the elastic spin ($\underline{W} = \underline{W}^e$). The internal state variable rate Eqs. (4) and (5) are functions of the observable variables (temperature, stress state, and rate of deformation). In Eq. (1), the elastic Lame constants are denoted by λ and μ. The elastic rate of deformation ($\underline{D}^e$) results when the total deformation ($\underline{D}$), which is defined by the boundary conditions, is subtracted from the inelastic flow rule as shown in Eq. (2).

The scalar parameter, D, in the BCJ equations is related to the void volume fraction and is often called damage. Because we are performing micromechanical simulations within this study, we desire that the material be dense for most of the calculations. As such, we nominally make $D = 0$. However, we show some results later in which we assume a small amount of porosity (0.0001) within the material along with the larger voids.

The independent variables for the inelastic rate of deformation are given in Eq. (3) as the stress, temperature, and internal state variables. The deviatoric inelastic flow rule, $\underline{D}^{\text{in}}$, is a function of the temperature, the kinematic hardening internal state variable ($\underline{\alpha}$), the isotropic hardening internal state variable (R), the volume fraction of damaged material (D), and the functions $f(T)$, $V(T)$, and $Y(T)$, which are related to yielding with Arrhenius-type temperature dependence. The function $Y(T)$ is the rate-independent yield stress. The function $f(T)$ determines when the rate-dependence affects initial yielding. The function $V(T)$ determines the magnitude of rate-dependence on yielding. These functions are determined from isothermal compression tests with different strain rates and temperatures,

$$V(T) = C_1\exp(-C_2/T),\ Y(T) = C_3\exp(C_4/T), f(T) = C_5\exp(-C_6/T). \tag{6}$$

The kinematic hardening internal state variable, $\underline{\alpha}$, reflects the effect of anisotropic dislocation density, and the isotropic hardening internal state variable R, reflects the

effect of the global dislocation density. As such, the hardening Eqs. (4) and (5) are cast in a hardening-recovery format that includes dynamic and static recovery. The anisotropic hardening modulus is $h(T)$, and the isotropic hardening modulus is $H(T)$. The functions $r_s(T)$ and $R_s(T)$ are scalar in nature and describe the diffusion-controlled static or thermal recovery, while $r_d(T)$ and $R_d(T)$ are scalar functions describing dynamic recovery. Hence, the two dominant types of recovery that are exhibited by populations of dislocations are captured in the model. The temperature dependent hardening-recovery parameters are given as

$$r_d(T) = C_7 \exp(-C_8/T) \tag{7}$$

$$h(T) = C_9 - C_{10} T \tag{8}$$

$$r_s(T) = C_{11} \exp(-C_{12}/T) \tag{9}$$

$$R_d(T) = C_{13} \exp(-C_{14}/T) \tag{10}$$

$$H = C_{15} - C_{16} T \tag{11}$$

$$R_s(T) = C_{17} \exp(-C_{18}/T). \tag{12}$$

The BCJ material constants $(C_1 - C_{18})$ were determined from quasi-static compression tests of 6061T6 aluminum and 304L stainless steel at different temperatures. Fig. 2 shows a comparison of the model and experimental results. Table A1 in the appendix lists the model constants used in our calculations. The FEM dense stress–strain curves arise from single element calculations, and the FEM porous stress-strain curves arise from simulations with many elements in which a void was included in the center. The final dropoff for the FEM porous simulations in Fig. 2a occurs because the void has grown such that it affects the overall stress–strain response of the aggregate material. Fig. 2 serves to confirm that the plasticity model accurately represents the material behavior.

3. Results and discussion

In this section, we discuss some parametric effects in terms of displacement controlled boundary conditions: multiple voids versus one void, temperature effects, void configuration effects, type of element used (axisymmetric versus planar 2D), and ILDs. Under the force controlled boundary conditions, we discuss constant stress triaxiality conditions and compare 6061T6 aluminum to 304L stainless steel.

3.1. Displacement controlled boundary conditions

Displacement, or strain, controlled boundary conditions are first examined as many experimental tests (cf. Lu, 1998) are performed in that manner. Applied strain rates were imposed under quasistatic conditions at 0.001/s.

3.1.1. Multiple voids

One major finding of this study is that when multiple voids are present within a dense ductile material, the void growth rate is greater than for a one void material with the same initial void volume. Figs. 3–5   illustrate this point for different
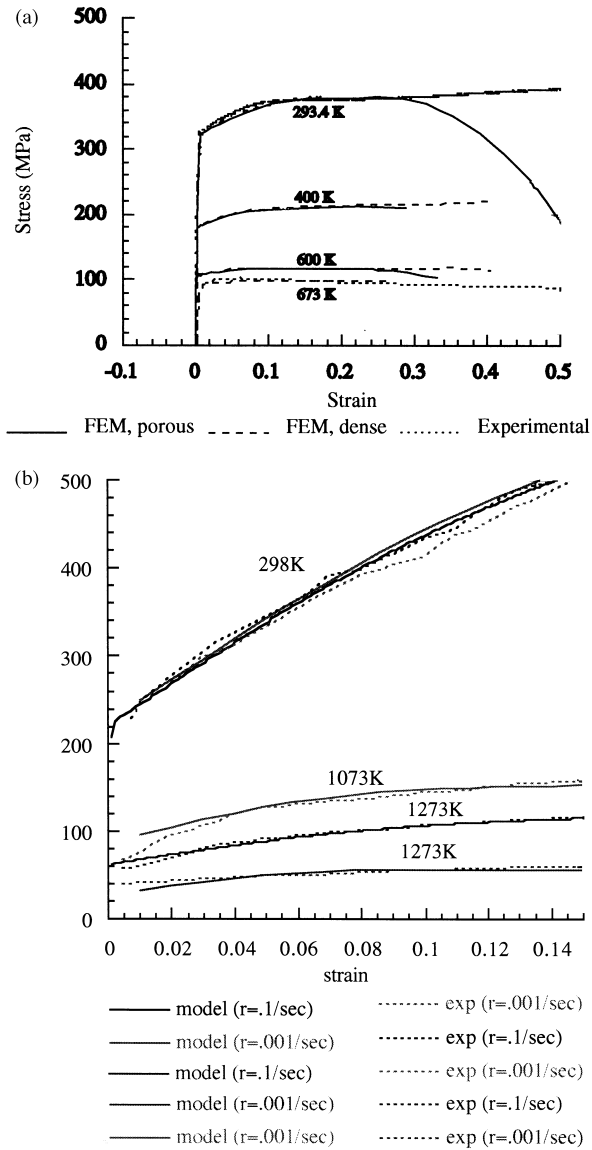

Fig. 2. (a) True stress–strain plots comparing the experimental data and BCJ plasticity model for pourous and dense 6061T6 aluminium at different temperatures and a strain rate of 0.001/s. (b) True stress–strain plots comparing the experimental data and BCJ plasticity model for porous and dense 304L stainless steel at different temperatures and a strain rate of 0.1/s.

boundary conditions and element types. Fig. 3 illustrates that for either the axisymmetric or planar 2D calculations, the material with two voids that had an ILD of one diameter always incurred a higher void growth rate than the material with only one void under biaxial stretching at 298 K. Fig. 4 demonstrates the same trend for plane strain boundary conditions. Fig. 5 also demonstrates the same trend for the uniaxial calculations although less pronounced, regardless of the void orientation with the straining direction. Although not obvious in Fig. 5, for strains beyond 35%, a void growth rate difference between the two void and one void material occurred for the axisymmetric calculations. This void growth enhancement in the multiple void material occurs because the free surface of the neighboring void introduces a local stress concentration and plastic strain enhancement in the ligament between the voids. The ligament stress concentration and plastic strain enhancement encourages the voids to grow larger and toward each other at a rate that is higher than if they were alone. The significance of the axisymmetric versus planar 2D calculations will be discussed later.

3.1.2. Temperature effects

Another major finding of this study is that as the temperature increases, the void growth rate is greater for a material with two voids than for a material with one
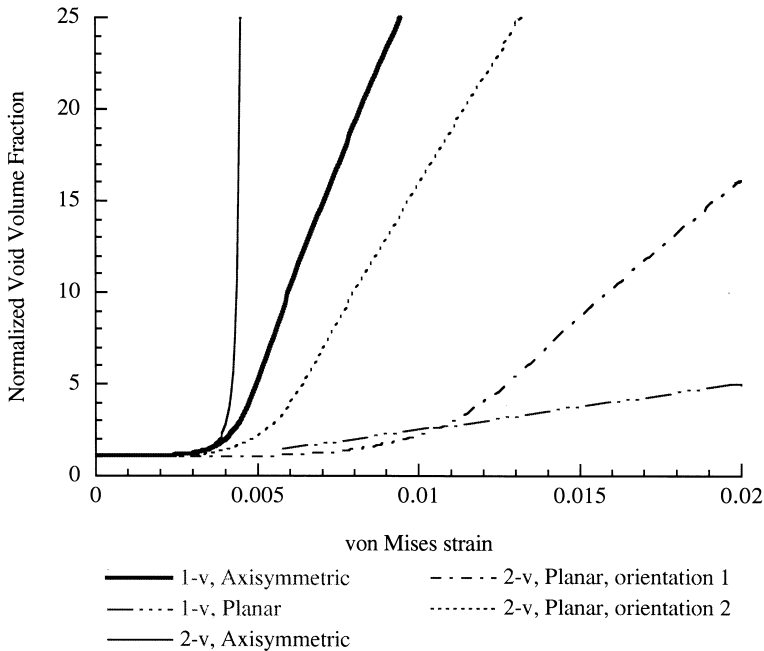

Fig. 3. Void volume fraction normalized by the void volume fraction versus von Mises strain illustrating the two void aluminium material will experience greater void growth than the one void case given the same initial void volume fractions. The boudary condition in this case is biaxial (stretch forming) displacement boundary conditions at room temperature ($\delta r / \delta a = 0.5$).
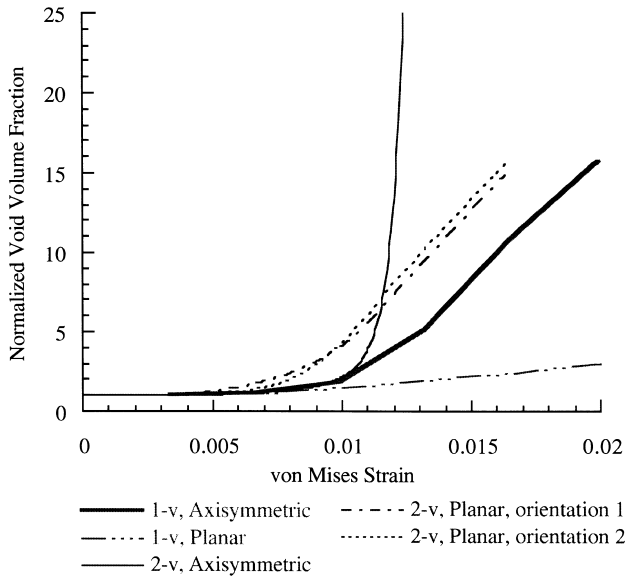
Fig. 4. Void volume fraction normalized by the initial void volume fraction versus von Mises strain illustrating the two void aluminium material will experience greater void growth than the one void case given the same initial void volume fractions. The boundary condition in this case is plane strain displacement at room temperature ($\delta r/\delta a = 0.0$).
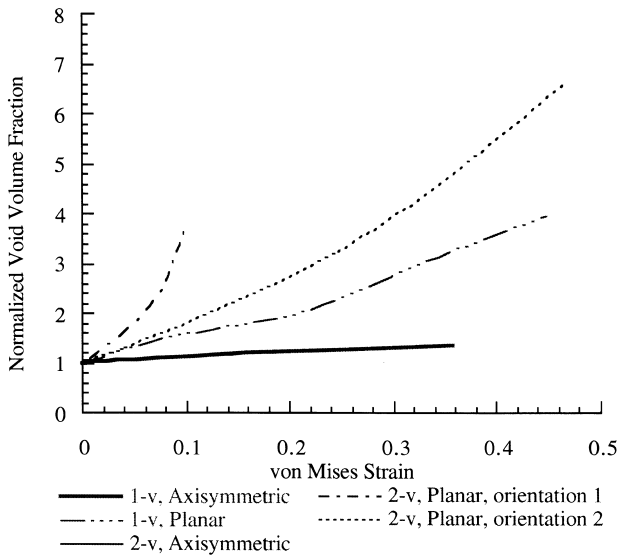

Fig. 5. Void volume fraction normalized by the initial void volume fraction versus von Mises strain illustrating that the two void aluminium material will experience greater void growth that the one void case given the same initial void volume fractions. The boundary condition in this case is uniaxial displacement boundary conditions at room temperature ($\delta r/\delta a \sim -0.3$).

void. For example, Fig. 6a and b show the normalized void volume fraction as a function of strain for axisymmetric, 6061T6 aluminum with two voids and one void, respectively. Fig. 6 shows that the one void material experienced void growth in an almost linear fashion, whereas the two void material experienced exponential growth. Other calculations showed that material with two voids always grew faster
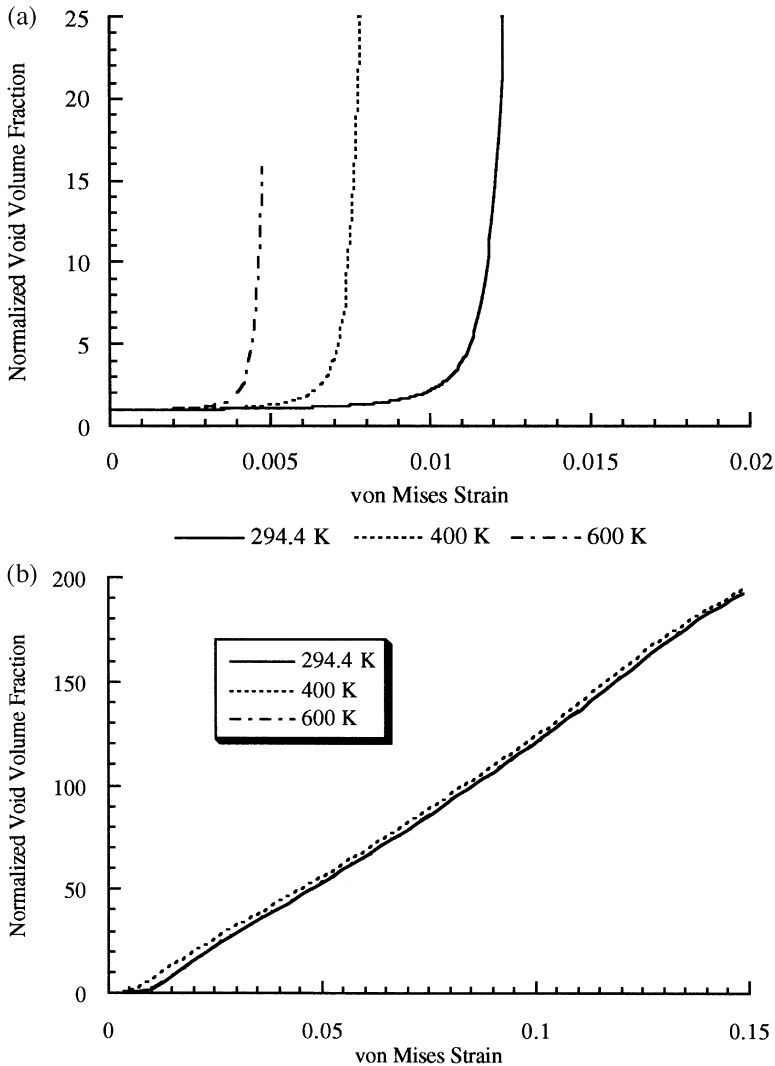

Fig. 6. (a) Void volume fraction normalized by the initial void volume fraction versus von Mises strain illustrating the greater void growth occurs as the temperature increases. The boundary condition is plane strain in the axisymmetric geometry with two void aluminium material ($\delta r/\delta a = 0.0$). (b) Void volume fraction normalized by the initial void volume fraction versus von Mises strain illustrating the greater void growth occurs the temperature increases. The boundary condition is plane strain in the axisymmetric geometry with one void aluminium material ($\delta r/\delta a = 0.0$).

than one void and this occurred for other boundary conditions, materials, and geometries as well.

The difference in void growth for one and two void material evokes the question, ''Why is there such a difference?'' Voids grow in ductile metals based on the level of stress triaxiality, defined here as the hydrostatic stress divided by the deviatoric stress, and plastic deformation (cf. Cocks and Ashby, 1980, 1982). In the one void material, the stress triaxiality remains essentially constant for the different temperatures although the total stress decreases as temperature increases. However, the plastic deformation increases as temperature increases, yet the one void material experiences about the same void growth up to approximately 15% strain independent of temperature. This result implies that the plastic deformation is less influential on void growth than the stress triaxiality for the one void material. Although not shown in Fig. 6b, when the von Mises strain level reached 30% for the one void material, the void grew at a different rate at different temperatures. At these larger strains, the plastic deformation played an increased role in promoting void growth. Fig. 7 shows contour plots of effective plastic strain at the same applied strain for two different temperatures of the two void material. Fig. 7 shows that the effective plastic strain for the 600 K two void material is an order of magnitude higher than for the 294 K material. As such, the large difference of void growth rates from one void material versus two void material is a function of the competing roles of the plastic deformation and stress triaxiality.

3.1.3. Void configuration effects

When considering the axisymmetric and planar 2D elements, different displacement boundary conditions, and different orientations of void pairs (see Fig. 1b and
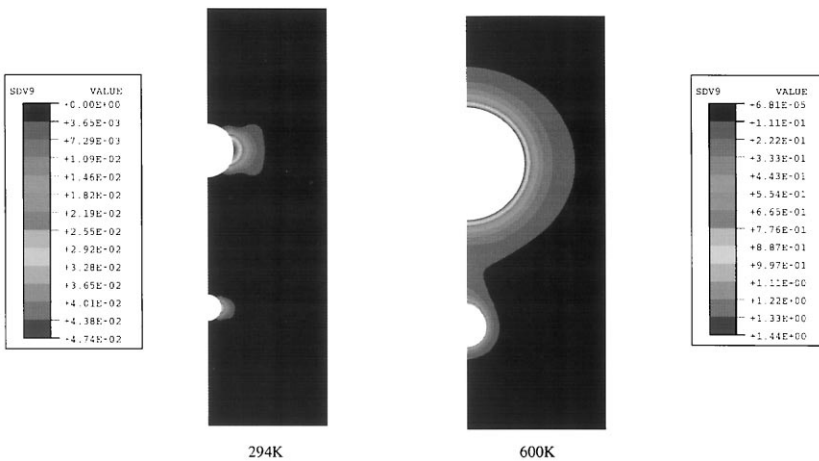

Fig. 7. Effective platic strain contours at the same snapshot in time illustrate the increase in plastic deformation as the temperature increases. This increase in plastic deformation enhances void growth. The boundary condition is plane strain, axisymmetric geometry with the two void aluminium material ($\delta r/\delta a = 0.0$).

c), we observe no distinguishable void growth trends. For our discussion, we specify "Orientation 1" as that defined in Fig. 1c and "Orientation 2" as that specified in Fig. 1b.

Fig. 8 shows the normalized void volume fraction as a function of strain for uniaxial straining (planar geometry) at various temperatures for 6061T6 aluminum. One can see that at all temperatures, "Orientation 2" experiences enhanced void growth over "Orientation 1." One might expect this result because the stress concentration is highest on the plane perpendicular to the loading axis. This larger stress increases the stress triaxiality. However, when considering other boundary conditions, the orientation influence changes.

For the highly constrained simulation in which a plane strain boundary condition was imposed on a planar 2D mesh, the void growth was quite similar between the two different void orientations at various temperatures as shown in Fig. 9. Because the zero displacement constraint is placed on the vertical faces, a tensile stress on the order of the loaded tensile stress arises in the perpendicular direction from Poisson's effect.

In Fig. 10, we see that the 6061T6 aluminum with "Orientation 2" experiences more void growth than the material with "Orientation 1" under the biaxial loading condition. This response was expected because biaxial straining was prescribed in a 2:1 ratio in which radial direction straining was higher than the axial direction. As mentioned earlier, this causes a stress concentration perpendicular to the direction
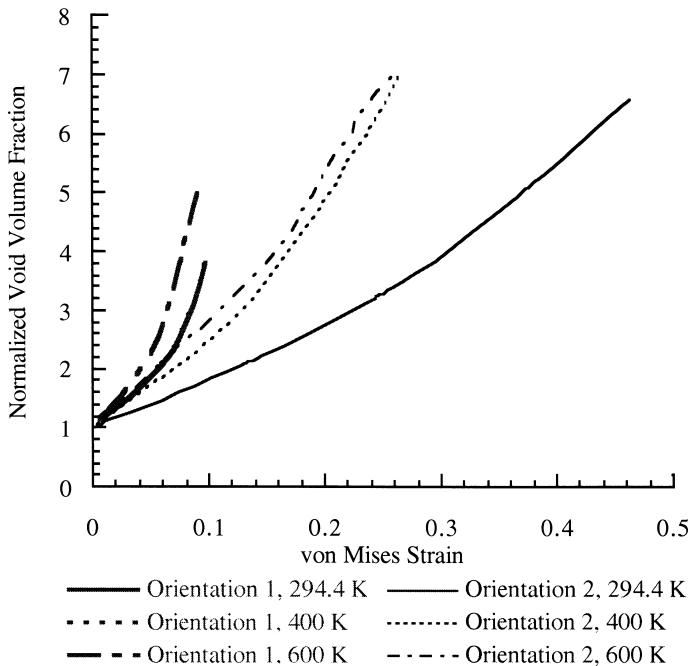

Fig. 8. Void volume fraction normalized by the initial volume fraction versus von Mises strain illustrating the effects of two void orientations in the uniaxial straining (plannar geometry) at various temperatures for 6061T6 aluminium ($\delta r/\delta a \sim -0.3$).

of the highest remote applied strain. The stress concentration encourages void growth in the perpendicular direction.

Although no clear void growth trends exist between the different void pair orientations, two definite observations can be made: (1) regardless of the void pair orientation, the two void material always experienced enhanced void growth over the one void material, and (2) the combination of the stress triaxiality and plastic deformation determines the extent of void growth.

Under the boundary conditions analyzed, the material with two voids at the highest temperature promoted the most void growth. However, under uniaxial straining, an interesting trend occurs when comparing the progression of void volume fraction when the two voids are colinear with the applied strain or perpendicular to the applied strain. Fig. 11 shows that for the two void material that is colinear with the applied strain, the 600 K material incurs higher void growth than the 294.4 K material, but the 400 K material is only slightly higher than the 294.4 K material. Now, Fig. 12 shows that for the two void material that is perpendicular to the applied strain, the 400 K material is only slightly less than the 600 K material. Apparently a threshold temperature related to relative spatial void geometry orientation exists at which the plastic deformation enhances void growth. In Fig. 11, the temperature threshold is between 400 and 600 K, whereas Fig. 12 shows that the
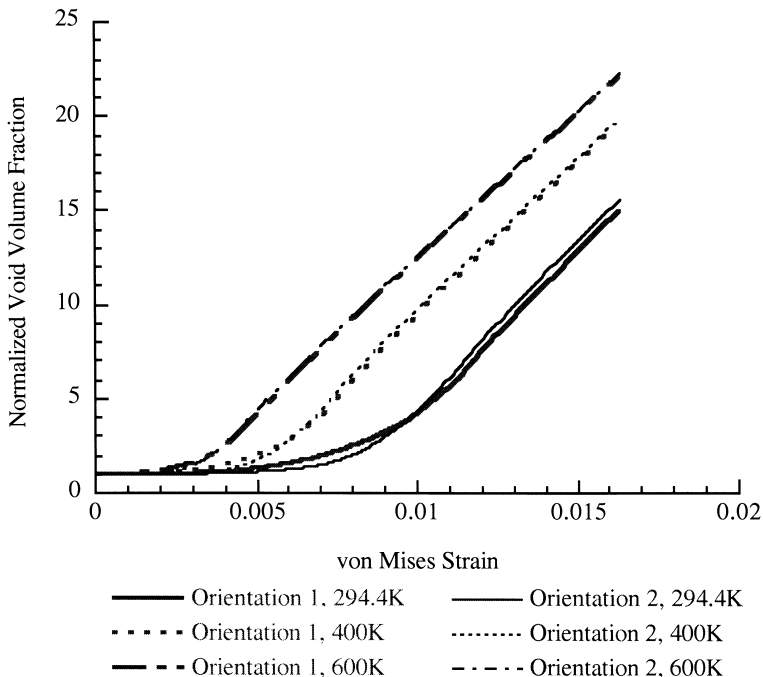

Fig. 9. Void volume fraction normalized by the initial void volume fraction versus von Mises strain illustrating that there are very slight differences for two void orientations in the "double" plane strining (planar geometry) at various temperatures for 6061T6 aluminium ($\delta r/\delta a = 0.0$).
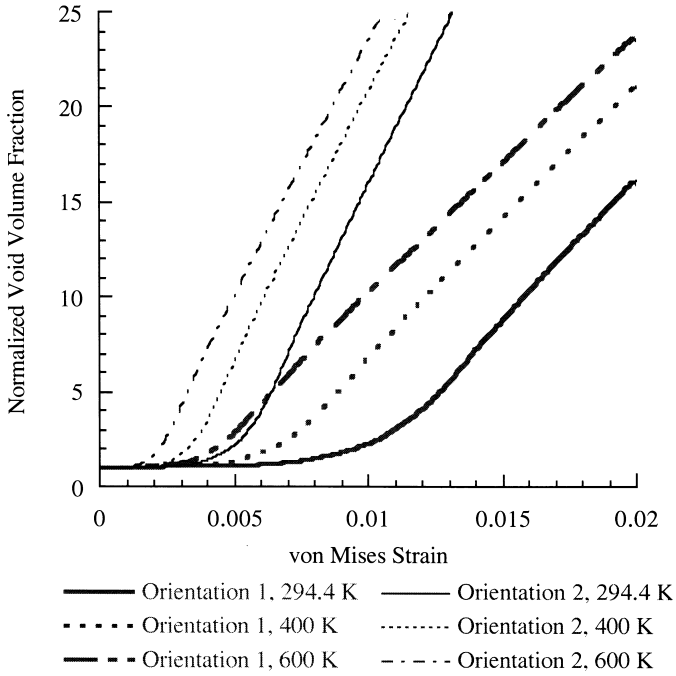
Fig. 10. Void volume fraction normalized by the initial void volume fraction versus von Mises strain illustrating the effects of two void orientations in the biaxial stretching (planar geometry) at various temperatures for 6061T6 aluminium ($\delta r/\delta a = 0.1$).
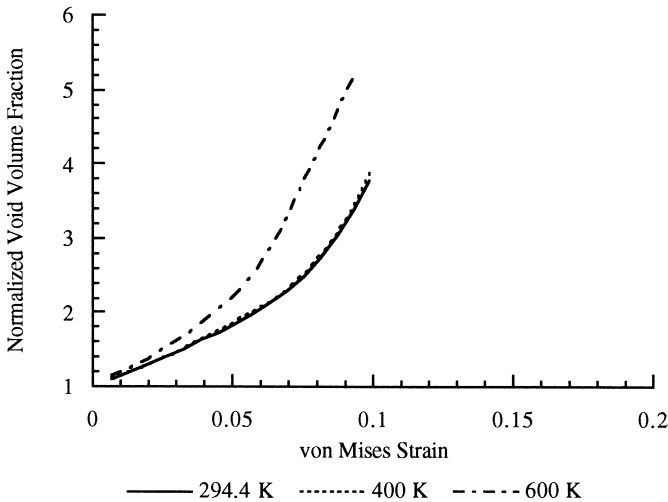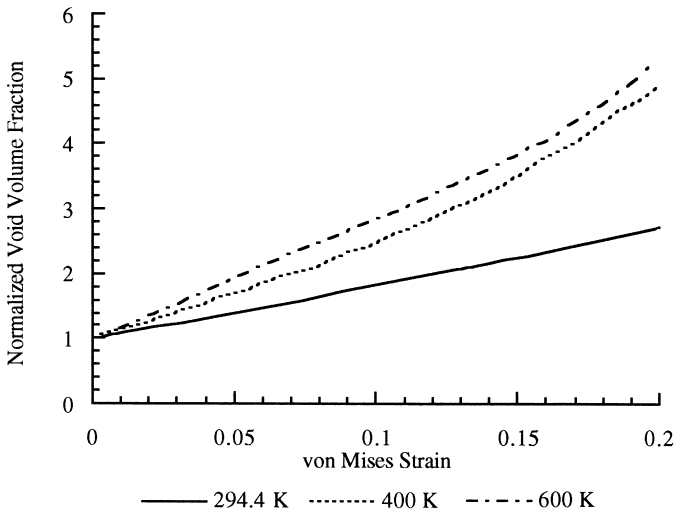

Fig. 11. Void volume fraction normalized by the initial void volume fraction versus von Mises strain for the two void case in orientation 1, axisymmetric, uniaxial conditions illustrates the closeness of void growth at 294.4 and 400 K for 6061T6 aluminium ($\delta r/\delta a \sim -0.3$).

Fig. 12. Void volume fraction normalized by the initial void volume fraction versus von Mises strain for the two void case in orientation 2, axisymmetric, uniaxial conditions illustrates the closeness of void growth at 400 and 600 K for 6061T6 aluminium ($\delta r/\delta a \sim -0.3$).
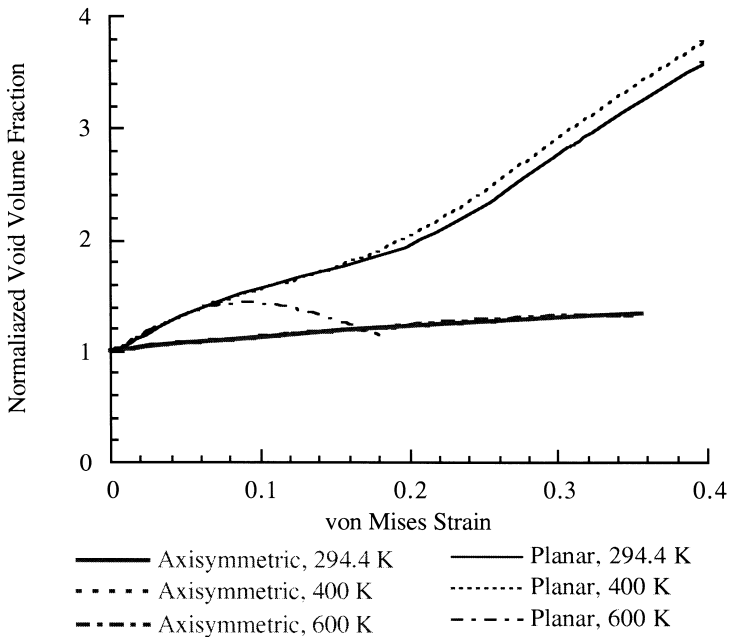

Fig. 13. Void volume fraction normalized by the initial void volume fraction versus von Mises strain illustrating that under uniaxial straining of the one void case, the planar geometry allows more void growth than the axisymmetric geometry at various temperatures.

temperature threshold is between 294.4 and 400 K. More finite element simulations are needed to systematically determine the threshold as a function of temperature and void configuration, but a trend is evidenced.

3.1.4. Type of element used

Another aspect of this study shows the relative importance of the type of element used (planar 2D and axisymmetric) on void growth. Fig. 13 shows the void growth rate for the one void material. (The planar 2D calculation for 600 K will be discussed later because a shear band formed.) Fig. 14 shows the void growth rate for the two void material. In both figures, the planar 2D mesh incurred more void growth than the axisymmetric mesh for the uniaxial loading calculation. This occurs because the stress triaxiality (Fig. 15) and plastic deformation (Fig. 16) were larger for the planar mesh. In Fig. 15, the stress triaxiality is determined from the average over all the elements as an aggregate value and is shown for both the one void and two void material. Fig. 15 shows that the stress triaxialities were higher for the planar 2D calculations than for the axisymmetric calculations. Fig. 16 compares strain contours for the planar and axisymmetric calculations at the same applied strain (for the one void 6061T6 aluminum at 294.4 K temperature under uniaxial straining). In Fig. 16 the peak effective plastic strain for the planar mesh was calculated as 1.6 near the void, but the peak effective plastic strain for the axisymmetric mesh was calculated as 0.50 near the void. Hence, both the stress triaxiality and plastic deformation
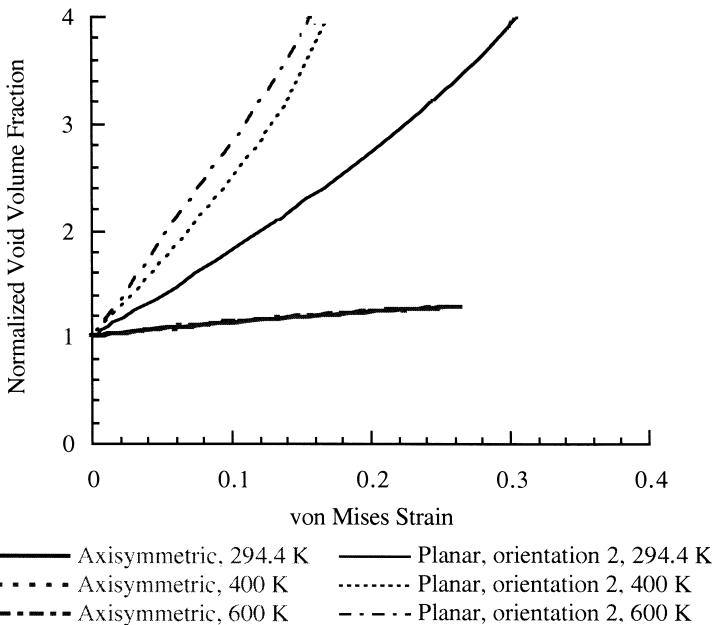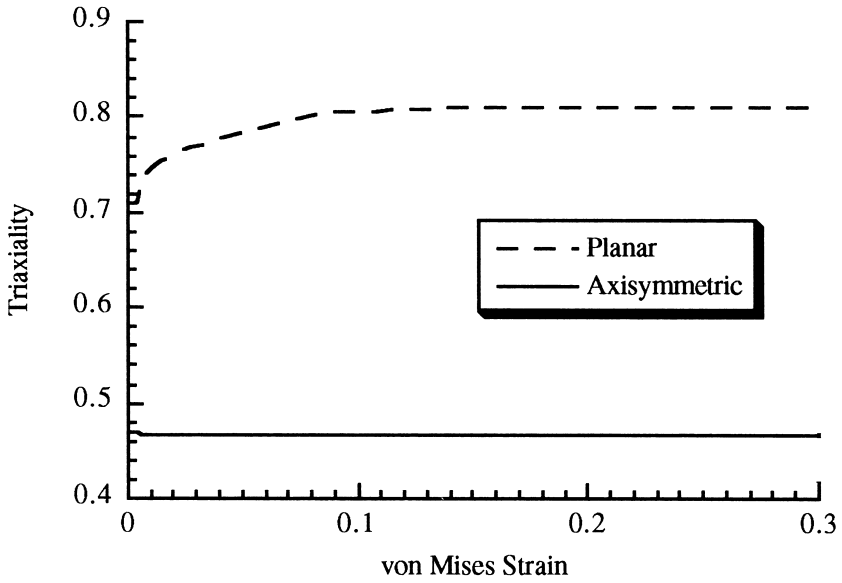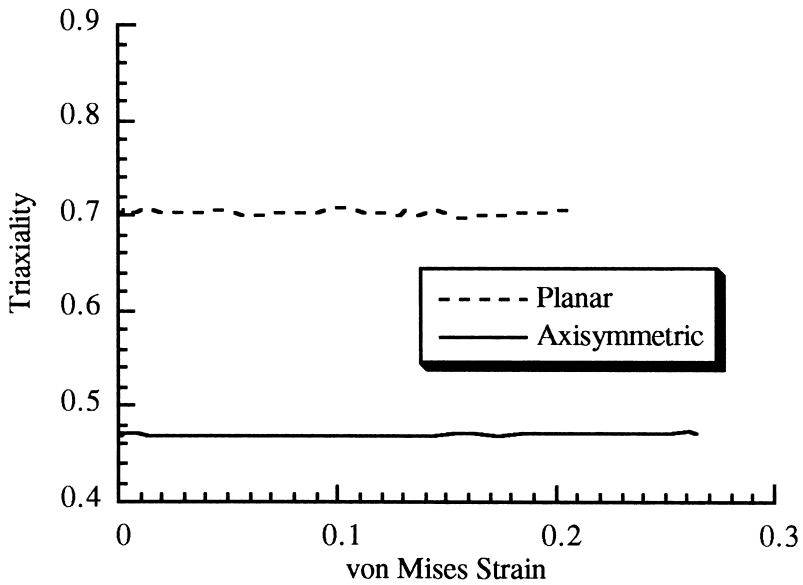

Fig. 14. Void volume fraction normalized by the initial void volume fraction versus von Mises strain illustrating that under uniaxial straining of the two void aluminium material, the planar geometry (orientation 2) allows more void growth that the axisymmetric geometry at various temperatures.

Fig. 15. Aggregate stress triaxialities versus von Mises strain shown that an increased stress triaxiality occurs for the planar geometry over the axisymmetric geometry, which corresponds to increased void growth in the uniaxial straining of the (a) one and (b) two void cases at room temperature for 6061T6 aluminium.
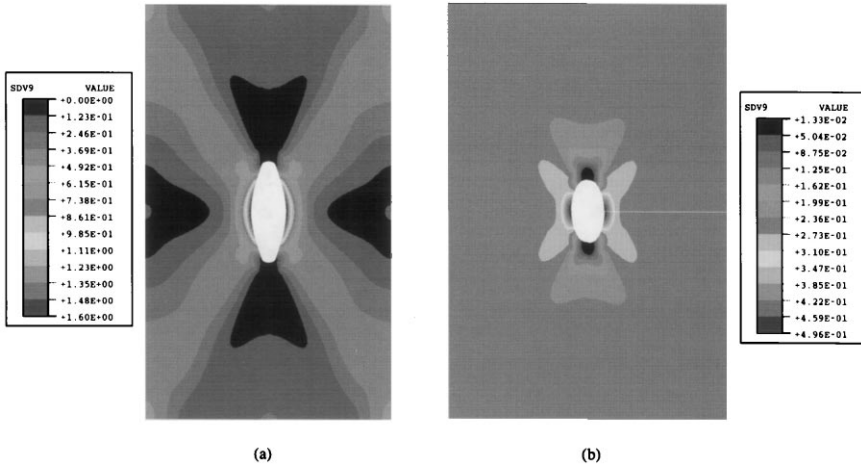
Fig. 16. Comparison of effective plastic strain contours of (a) planar and (b) axisymmetric geometries under uniaxial straining at the same time illustrates that the planar geometry incurs higher strains. The calculations were run at room temperature for the one void aluminium material.
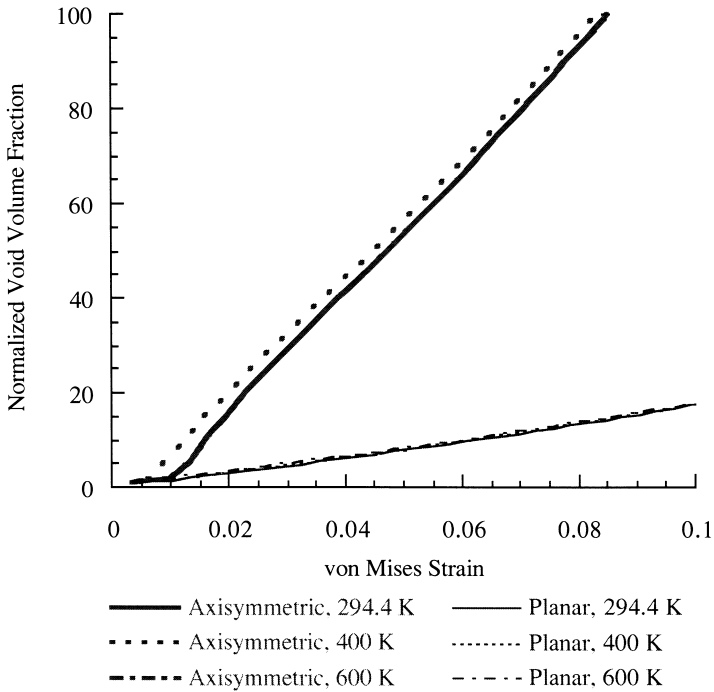

Fig. 17. Void volume fraction normalized by the initial void volume fraction versus von Mises strain illustrating that for the plane strain boundary condition of the one void aluminium material, the axisymmetric geometry allows more void growth at various temperatures ($\delta r/\delta a = 0.0$).

were higher for the planar mesh than for the axisymmetric mesh, thus inducing higher void growth.

The preceding paragraph relates to uniaxial loading. We will now see that for plane strain and biaxial conditions with one void and two void 6061T6 aluminum, the trend is opposite of the uniaxial condition. Fig. 17 for the plane strain calculation and Fig. 18 for the biaxial calculation show that the axisymmetric mesh allows higher void growth than the planar mesh for the one void material. Figs. 19 and 20 show similar results for the two void material. The corresponding stress triaxialities, as shown in Fig. 21, for both the planar 2D and axisymmetric calculations are similar in magnitude although the planar mesh gives a slightly higher value as deformation proceeds to larger strains. However, the plastic deformation is much higher for the axisymmetric calculation under these straining conditions and that is why voids grow faster. Fig. 22 shows that peak effective plastic strain is 332% for the axisymmetric calculation and about 50% for the planar calculation. This again shows that depending on the temperature and boundary conditions, void growth is dependent upon both the stress triaxiality and plastic deformation. At higher temperatures, the plastic deformation seems to be more important than the stress triaxiality. At lower temperatures, the stress triaxiality is more important than the plastic deformation. A critical temperature exists at which both the stress triaxiality and effective plastic strain have an equal amount of influence.
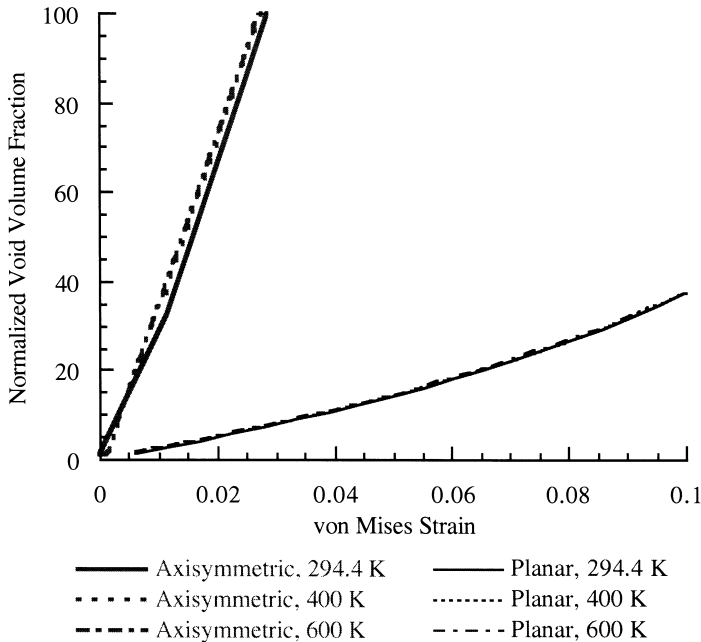

Fig. 18. Void volume fraction normalized by the initial void volume fraction versus von Mises strain illustrating that for the biaxial stretch boundary condition of the one void aluminium material, axisymmetric geometry allows more void growth than the planar geometry at various temperatures ($\delta r/\delta a = 1.0$).

3.1.5. Intervoid ligament distance (ILD) for void growth enhancement

Up to this point, the ILD was initially one void diameter. Brown and Embury (1973) noted that voids coalesce by impingement when they grow to a dimension in which the diameter is equal to the spacing. This assertion was based upon the observation that the void shapes did not change until they were one void diameter apart. Since Brown and Embury (1973) did not perform a detailed finite element study of various intervoid distances, they could not determine if the void growth rate was higher for ILDs greater than one diameter. Granted, a void may "spherically" grow until a void one diameter away is sensed, but the void growth rate could be higher before the strain level is achieved that changes the void shape. To study this, we performed different calculations by varying the ILD, as shown in Fig. 23, to determine a critical ILD. We define void coalescence as a point of deviation from single void growth. As such, we do not designate the onset of void coalescence when the shape changes, but when the growth rate changes from the one void case.

The parameters varied to study the ILD were temperature, boundary condition, type of element used, orientation of void pairs, and material (6061T6 aluminum and 304L stainless steel). A typical example is shown in Fig. 24 of the void growth in terms of void size normalized by the initial void size plotted versus the applied strain for a biaxial calculation at 294.4 K for 6061T6 aluminum. Fig. 24 illustrates that at strains below 0.0005, the one void result and the result for two voids with an ILD of
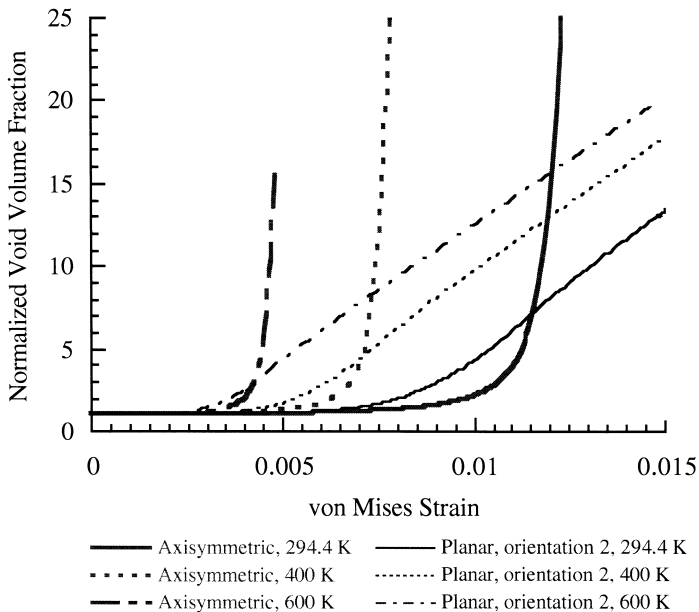

Fig. 19. Void volume fraction normalized by the initial void volume fraction versus von Mises strain illustrating that for the plane strain boundary condition of the two void aluminium material, the axisymmetric geometry allows more void growth than the planar geometry (orientation 2) at various temperatures ($\delta r / \delta a \sim -0.3$).

six diameters are similar. From this result, we assert that if the ILD is less than six diameters at the beginning of loading or during loading at some strain level, we claim that coalescence has occurred.

Fig. 25 summarizes the results showing that a critical ILD for coalescence is dependent on temperature, geometric condition, orientation, boundary condition, and material work hardening rate. The results indicate that for macroscale modeling of void coalescence microstructural quantification of the initial void distribution is needed. For engineering materials, coalescence is a continual process starting at the beginning of deformation as different size voids grow together before final failure occurs. The void growth functions often used in finite element simulations (cf. McClintock, 1968; Rice and Tracey, 1969; Cocks and Ashby, 1980, 1982) are based on a single void growing and need modification to account for coalescence to accurately model engineering materials.

3.1.6. Shear banding experienced in some calculations

One last result needs attention related to Fig. 13. Fig. 13 shows that the uniaxial, planar 2D calculation at 600 K experienced a void volume drop-off at about 7% von Mises strain. The reason for this decreasing void volume fraction is that the deforming material localized and a shear band developed. Fig. 26 shows a color contour plot of the shear strain after localization illustrating the shear bands that
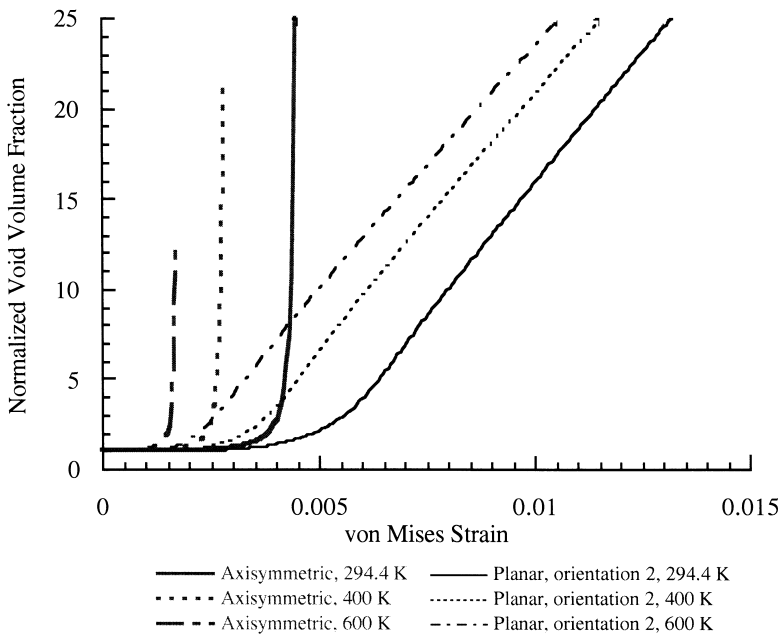

Fig. 20. Void volume fraction normalized by the initial void volume fraction versus von Mises strain illustrating that for the biaxial stretch boundary condition of the two void aluminium material, the axisymmetric geometry allows more void growth that the planar geometry (orientation 2) at various temperatures ($\delta r / \delta a = 1.0$).

arose during the calculation. Because of the different mode of failure expressed here, analysis of void coalescence by impingement is not pertinent.

3.2. Force controlled boundary conditions

Since the calculations in Section 3.1 were displacement controlled, the evolving stress triaxiality can make it difficult for macroscale modeling of coalescence. Therefore, we examine the multiple void effects, temperature effects, and material work hardening effects in the context of constant applied stress triaxiality. Force controlled boundary conditions are actually used to determine the stress state. Constant triaxialities ranging from 0.3 (representing uniaxial tension) to 10 were applied. Stress triaxialities up to 10 can potentially be reached in shock environments.

3.2.1. Constant stress triaxiality discussion

The void growth enhancement trends observed for the constant stress triaxiality calculations are similar to those of the displacement controlled boundary value problems. Fig. 27 shows the void volume fraction normalized by its initial void volume fraction as a function of von Mises strain for finite element simulations in which the triaxialities were varied for 6061T6 aluminum with one and two voids at 294.4 K in the axisymmetric geometry. From the displacement controlled two void
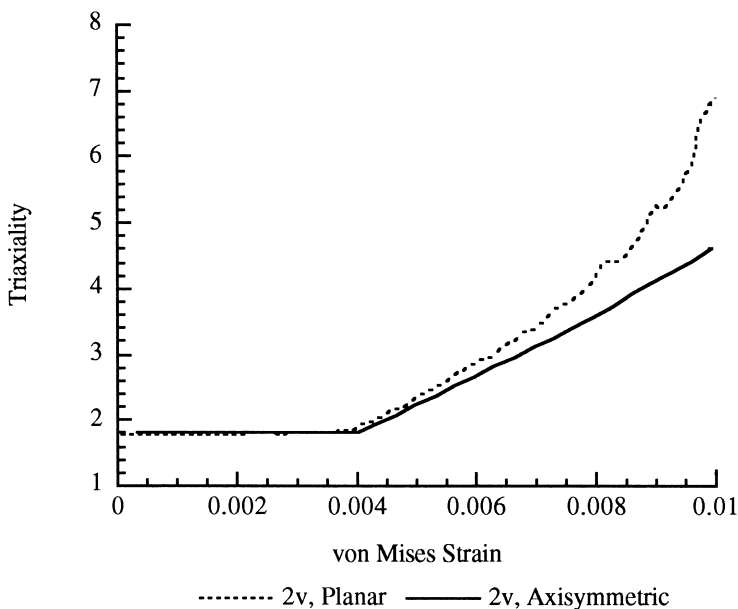
Fig. 21. Aggregate stress triaxialities versus von Mises strain shows that an increased stress triaxiality occurs for the planar geometry over the axisymmetric geometry for the biaxial stretching boundary condition for 6061T6 aluminium.

simulations, we observed that the void growth was always enhanced in the presence of two voids. Fig. 27 agrees with stress triaxialities above 0.3. Note that stress triaxialities can be fairly small ($\sim$2) and still a large difference in void growth occurs. Fig. 27 also reveals the greater difference in void volume increase as the stress
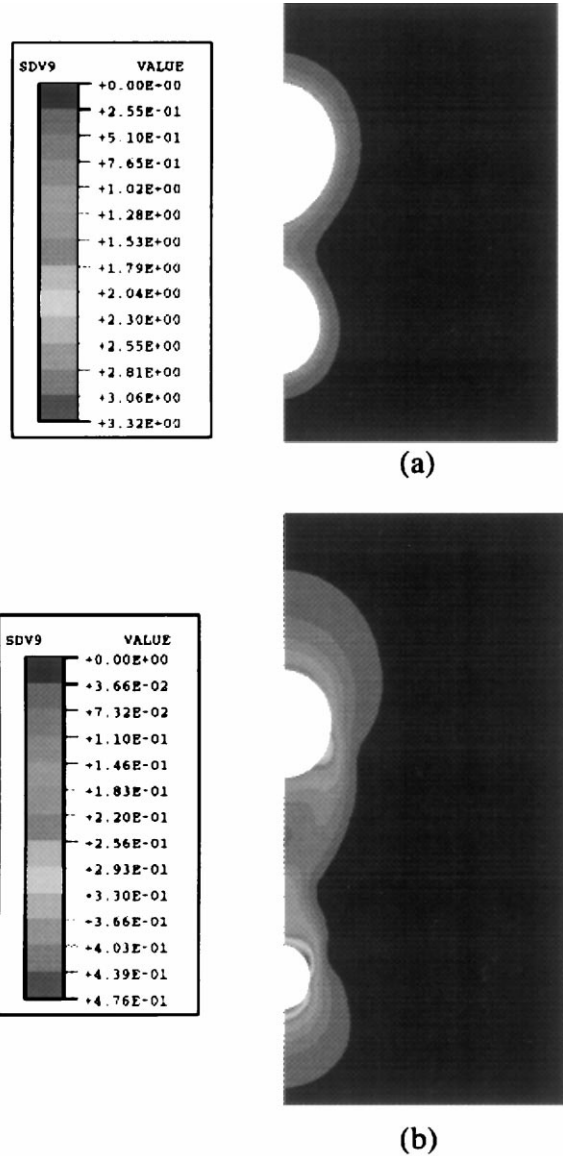

Fig. 22. Effective plastic strain contours illustrate the differences in plastic deformation for the (a) axisymmetric and (b) planar calculations. This typical response is shown for the room temperature, two void 6061T6 aluminium under biaxial straining.
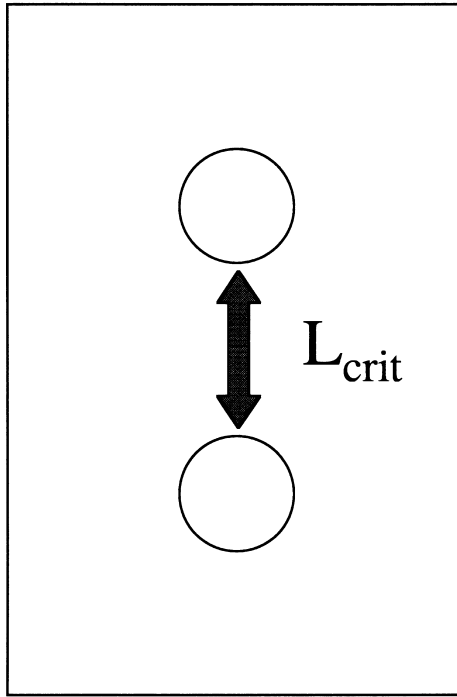
Fig. 23. The critical intervoid ligament distance is examined by determination of enhanced void growth. The critical L determines if the distribution of voids can be considered dilute or concentrated.
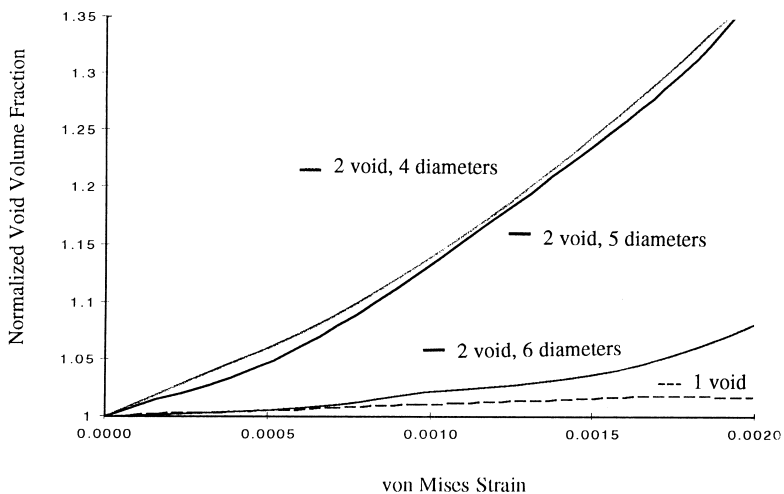

Fig. 24. The critical intervoid distances were determined by comparing responses of multiple voids growing to the single void case. The six void diameter case was identical to the single void case below a strain of 0.0005. This calculation was a biaxial, axisymmetric calculation at room temperature for 6061T6 aluminium.
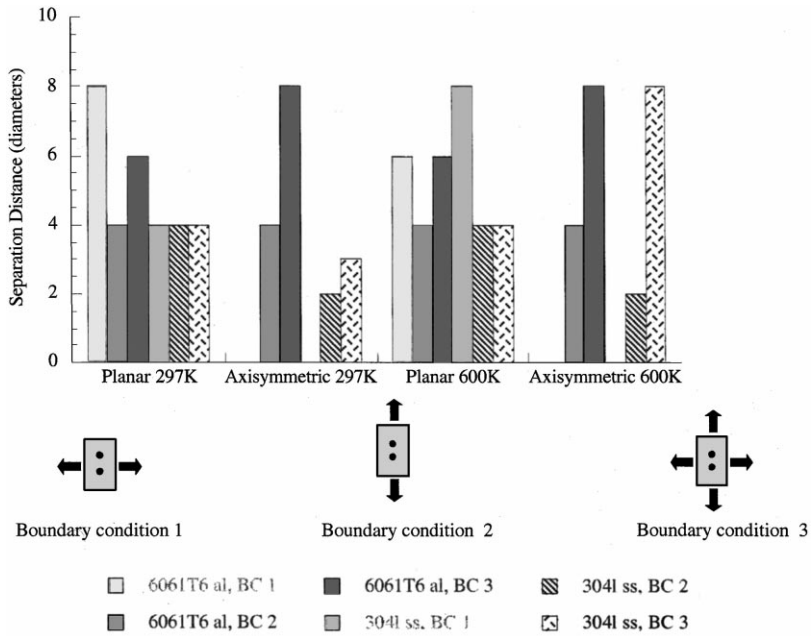
Fig. 25. The critical intervoid distances determined to enhance void growth. The critical length, *L*, is determined for different loading conditions, temperatures, materials, and void configurations.
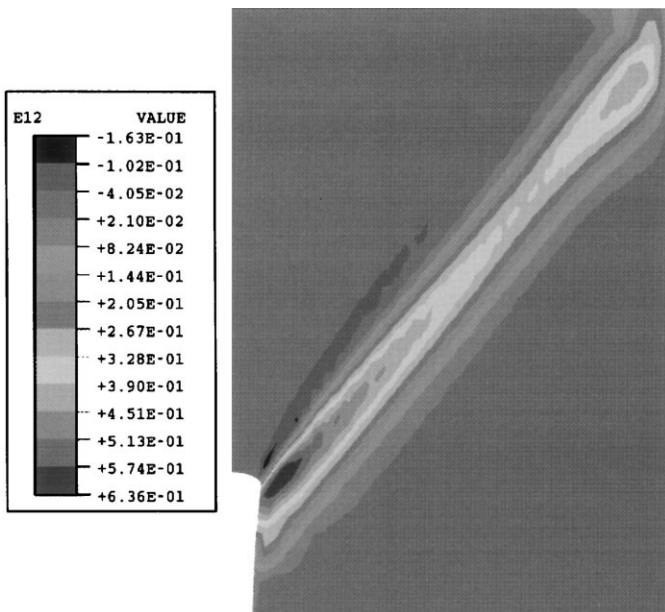

Fig. 26. Illustration of shear band from contour plot of shear strain for one void, uniaxial, planar 2D calculation at 600 K for 6061T6 aluminium.

triaxiality increases. For a one void material, at strains below 5%, the growth is almost linear and the nonlinearity does not occur until larger strains. For the two void material, the nonlinearity starts almost immediately at strains below 1% for stress triaxialities above 0.3. Above a stress triaxiality of five, the void growth rate does not change much for the two void material.

Fig. 28 shows data similar to Fig. 27 but for 304L stainless steel. Note that the character of the one void material is similar to the two void material. The difference between the 304L stainless steel and 6061T6 aluminum for the one and two void materials can be attributed to the work hardening rate differences. For 6061T6 aluminum, the work hardening rate is much less than for 304L stainless steel. Therefore, once a large enough stress surrounding a void occurs, the almost perfectly plastic aluminum matrix plastically deforms at a higher rate than the 304L stainless steel. This is demonstrated in Fig. 29, which shows the same applied strain level comparing the effective plastic strain for 304L stainless steel and 6061T6 aluminum.

Figs. 27 and 28 display void growth data that illustrates how a definite transition exists from linear void growth to exponential void growth as the stress triaxiality
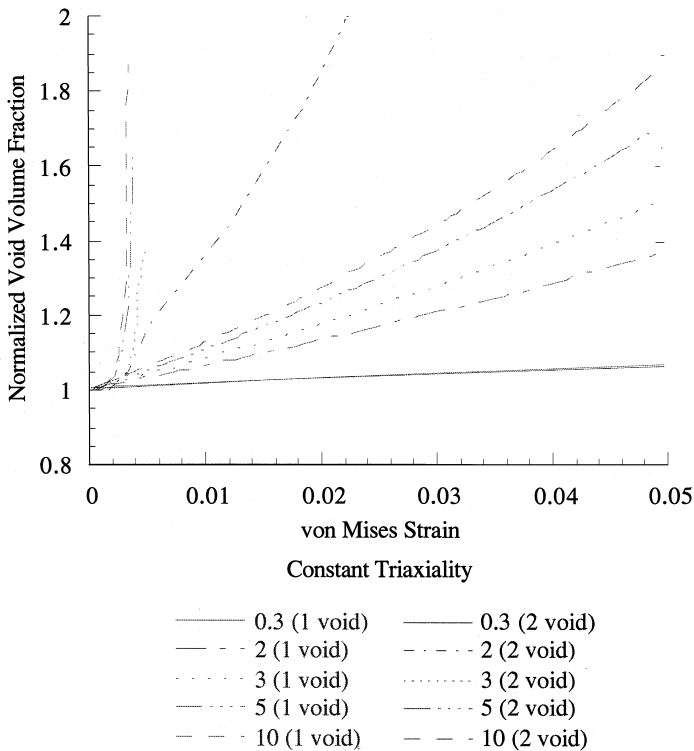

Fig. 27. Void volume fraction normalized by the initial void volume fraction versus von Mises strain illustrating the increase in void growth as the stress triaxiality increases for 6061T6 aluminium with two voids over one void. These calculations were performed under constant triaxialty conditions, at room temperature, and for the axisymmetric geometry.

increases for even one void material. Furthermore, the transition between void growth from a linear rate to an exponential rate is enhanced for a two void material. A void growth rate transition exists between the triaxialities of two and three for the 304L stainless steel with any number of voids. This transition has been observed previously by Lee and Dawson (1993) in which the Hart model was used instead of the BCJ model for an 1100 aluminum. For the one void 6061T6 aluminum, no distinct transition occurs between a triaxiality of two and three.

Another statement made earlier relating the displacement controlled calculations was that voids do not grow differently at different temperatures when only one void is present until large strains ($\sim$30%) are experienced. Fig. 30 confirms this statement as the constant triaxiality of 0.3 demonstrates the same trend. However, at higher stress triaxialities 6061T6 aluminum with one void can indeed experience enhanced void growth as the temperature increases. Fig. 31 shows void growth as a function of von Mises strain for a stress triaxiality of 10. Note that the strain levels are very small when the difference in void growth starts to appear.

Figs. 32 and 33 show normalized void volume fraction versus von Mises strain for stress triaxialities of two and 10, respectively. Both show void growth enhancement as temperature increases very similar to the manner of the displacement controlled boundary conditions.

Fig. 28. Void volume fraction normalized by the initial void volume fraction versus von Mises strain illustrating the increase in void growth as the stress triaxiality increases. For 304L stainless steel, there is no difference between the void growth for the one and two void case. These calculations were performed under constant triaxiality conditions, at room temperature, and for the axisymmetric geometry.
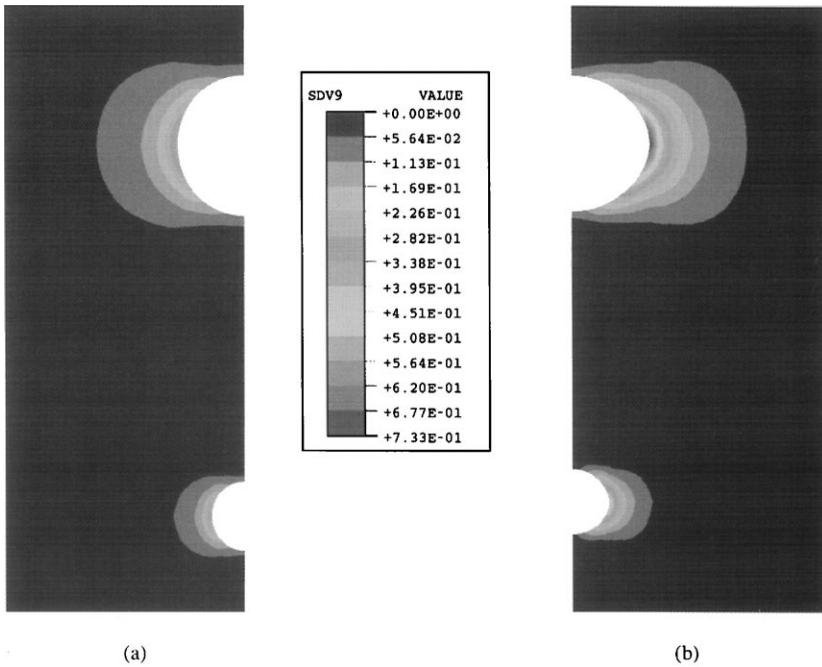
Fig. 29. Comparison of von Mises strain contours at the same external load and time for (a) 304L stainless steel and (b) 6061T6 aluminium. These calculations were performed under constant triaxiality ($X = 0.3$) conditions, with two voids with an axisymmetric geometry.
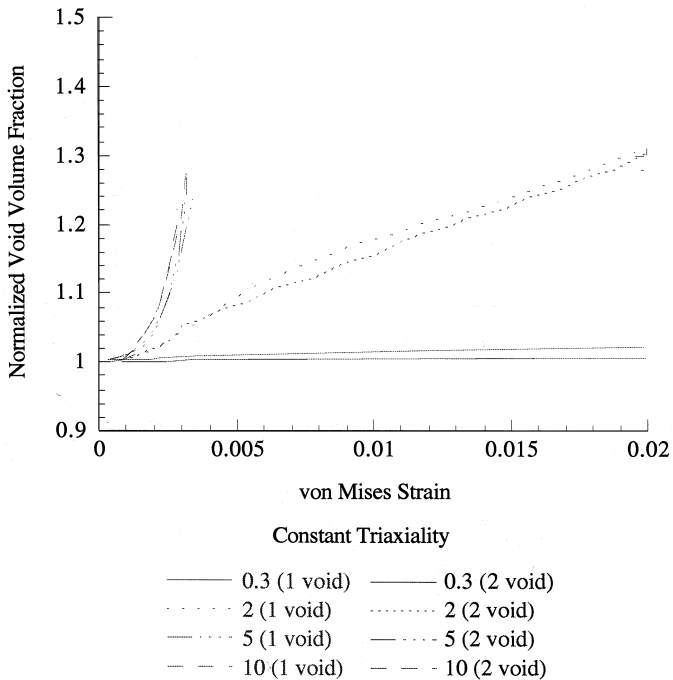

Fig. 30. Void volume fraction normalized by the initial void volume fraction versus von Mises strain illustrating the increase in void growth as the stress triaxiality increasing temperature. These calculations were performed on 6061T6 aluminium under constant triaxiality ($X = 0.3$) conditions, with one void, and for the axisymmetric geometry.

Fig. 31. Void volume fraction normalized by the initial void volume fraction versus von Mises strain illustrating the increase in void growth as the stress triaxiality increases for increasing temperature. These calculations were performed on 6061T6 aluminium under constant triaxility ($X = 10$) conditions, with one void, and for the axisymmetric geometry.
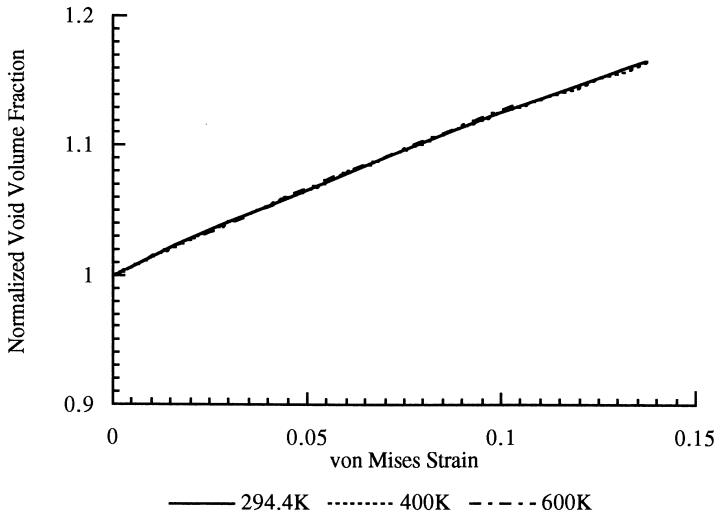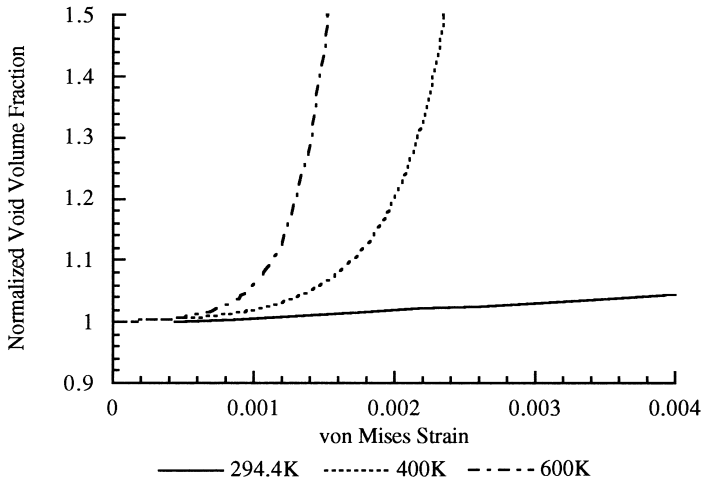

Fig. 32. Void volume fraction normalized by the initial void volume fraction versus von Mises strain illustrating the increase in void growth as the stress triaxiality increasing temperature. These calculations were performed on 340L stainless under constant triaxiality ($X = 2$) conditions, with one void, and for the axisymmetric geometry.

Fig. 34 shows normalized void volume fraction as a function of von Mises strain comparing 6061T6 aluminum and 304L stainless steel for one void and two void material at different temperatures and an applied stress triaxiality of 10. As Fig. 34 clearly shows, void growth in the 6061T6 aluminum experiences more temperature dependence than the 304L stainless steel. This is consistent with an earlier discussion that the work hardening rate is almost flat (perfect plasticity) for 6061T6 at 600 K, but for 304L stainless steel a positive work hardening rate still exists as exemplified in Fig. 2b.

Fig. 34 also addresses a question that is often asked regarding various materials, namely, "In which material do voids grow faster?" Based on these calculations, the answer to that question depends on the temperature. Since each material has its own temperature dependent yield stress and work hardening rate, voids do not always grow faster for one material over another. McClintock (1968) and Rice and Tracey (1969) showed that one void growth equations can be developed based upon the work hardening exponent of power law plasticity. As shown in Fig. 2, the work hardening rate is changed from one material to another and from one temperature to another. In particular, the 6061T6 aluminum experiences a much lower *change* in work hardening rate than the 304L stainless steel. At 294.4 K, the 304L stainless steel experiences more void growth at least at these small strain levels. Above 400 K,
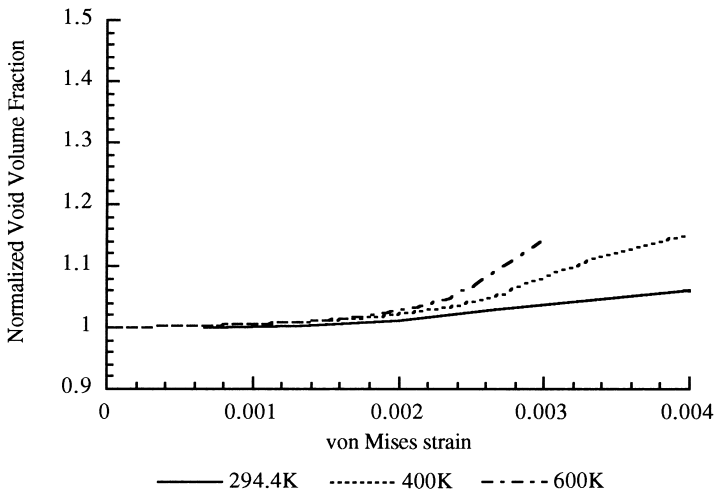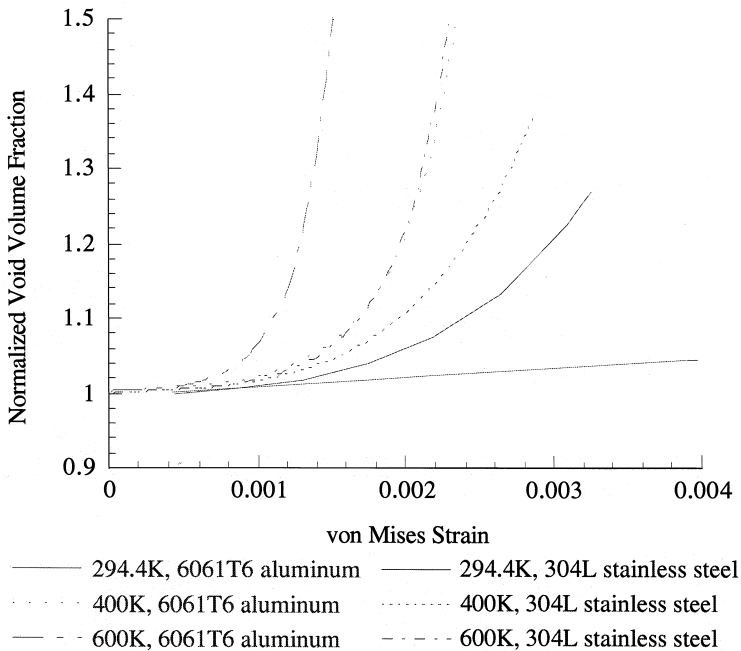

Fig. 33. Void volume fraction normalized by the initial void volume fraction versus von Mises strain illustrating the increase in void growth as the stress triaxiality increases for increasing temperature. These calculations were performed on 340L stainless steel under constant triaxiality ($X = 10$) conditions, with one void, and for the axisymmetric geometry.

the aluminum experiences a higher void growth. Hence, void growth depends on the work hardening rate and a multitude of parameters as demonstrated here: void configuration and distribution, number of voids, boundary condition, temperature, and strain rate.

3.2.2. Dense versus porous matrix

Up to now, the discussion has focused on large voids in a dense (pore free) metal. Fig. 35 shows a comparison of normalized void volume fraction versus von Mises strain in which one and two void configurations are modeled with and without a porous matrix metal. These 6061T6 aluminum calculations were performed under biaxial straining conditions at 294.4 K under a quasi-static strain rate. The porous aluminum essentially included an initial microporosity level of 0.0001 distributed evenly throughout the mesh. The result in Fig. 35 shows that for the two void configuration, the inclusion of microporosity did not enhance the void growth rate. However, for the one void material, the microporosity enhanced the growth of the larger pore over the one void material without microporosity. Interestingly, void growth rate for the one void material with microporosity was slightly lower than that of the two void material. This indicates that (i) the two larger voids dominate

Fig. 34. Void volume fraction normalized by the initial void volume fraction versus von Mises strain illustrating increasing temperature leads to increased void growth. 6061T6 aluminium experiences a stronger temperature dependent void growth than 340L stainless steel. However, we note that at room temperature 304L stainless steel experiences a slightly higher void growth than 6061T6 aluminium. These calculations were performed on 340L stainless steel and 6061T6 aluminium under constant triaxiality ($X = 10$) conditions, with one void, and for the axisymmetric geometry.

the response and interaction and the microporosity is essentially noise for the two void material and (ii) the microporosity distributed throughout mesh can enhance void growth much like a neighboring large void. Horstemeyer and Ramaswamy (2000) showed that the influence of microporosity on larger pores does indeed play a major role for void growth rates on single voids.

3.3. Potential strain rate effects

Not covered in the analyses thus far have been strain rate effects. Future studies are planned to assess this aspect. Budiansky et al. (1982) first showed that a decrease in the strain rate sensitivity parameter enhanced void growth from a single void in a dense solid. Briottet et al. (1996) showed a similar trend albeit less pronounced for a single void in a compressible solid. Benson (1993, 1995) from numerical simulations noted different locations of failure from clustering effects in high strain rate micromechanical simulations of different void configurations. One can reason based upon dislocation motion and interaction that void coalescence would occur in the opposite trend as that of the temperature trend. Further studies of strain rate effects are planned to quantify this effect, but let us consider a power law plasticity equation with strain rate and temperature effects,

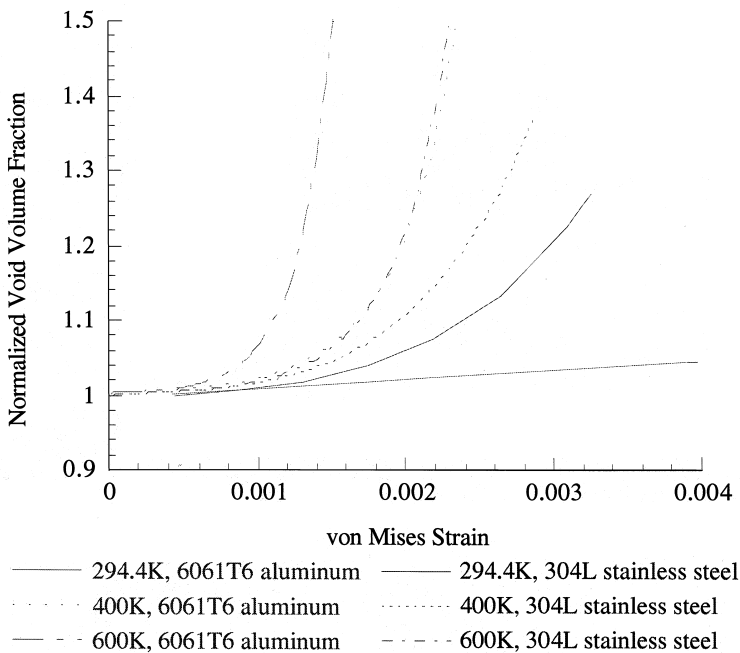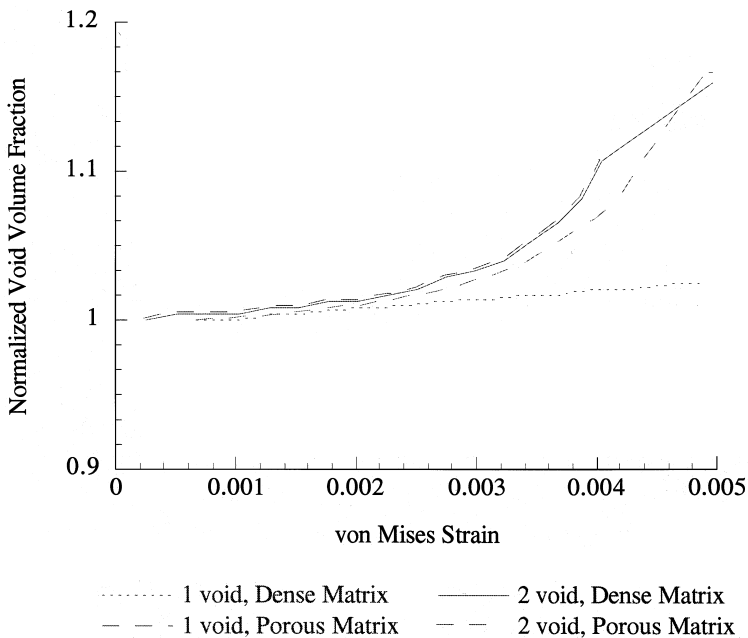Fig. 35. Void volume fraction normalized by the initial void volume fraction versus von Mises strain illustrating the differences between fully dense and porous material. These calculations were performed on 6061T6 aluminium under constant triaxiality ($X = 2$) conditions at room temperature for the axisymmetric geometry.

$$\sigma = A\varepsilon^n \dot{\varepsilon}^m \exp(-\Delta G/kT) \tag{13}$$

where the state of stress is a function of the Gibbs free activation energy G, temperature T, the Boltzmann constant k, the strain rate $\dot{\varepsilon}$, hardening exponent n, hardening coefficient A, and strain rate exponent m. Eq. (13) represents thermally activated dislocation glide past obstacles. Eq. (13) also reveals that as the temperature increases, the stress decreases, but as the strain rate increases, the stress increases. Hence, one can observe the inverse relation that temperature and strain rate have on the stress state. Because the stress state and strain state determine the void growth and coalescence rates, void growth and coalescence trends for increasing strain rates are anticipated to display the opposite trend than for increasing temperatures. Since void coalescence is enhanced at higher temperatures, we anticipate that void coalescence would be enhanced at lower strain rates. Conversely, since void coalescence is inhibited at lower temperatures, we anticipate that void coalescence would be inhibited at higher strain rates. This inhibited void coalescence is observed in spall tests, which occur at high strain rates and can induce stress triaxialities on the order of 10 (cf. Eftis et al., 1991; Zurek et al., 1997). Nemes and Eftis (1993) showed numerically for notch tensile bars that the place of final fracture occurs at different locations depending on the applied strain rate. One could expect this with temperature effects too (cf. Lu et al., 1998).

3.4. Suggestion for macroscale continuum modeling

In terms of continuum damage modeling, one must consider distribution effects of voids or at least a spatial dimension that relates neighboring voids as demonstrated by this numerical study. Experimental studies have shown this in a qualitative manner in the past (cf. Garrison and Moody, 1987). In particular, if the critical ILD is broached, then the continuum damage model should include this coalescence effect. One can cast this into an internal state variable framework, because the creation of new surface area is enhanced by coalescence. By assuming generalized normality, the Kelvin inequality of the Second Law of Thermodynamics is unconditionally satisfied (nonnegative intrinsic dissipation) and is expressed in the following equation

$$\underline{\sigma} : \underline{D}^{\mathrm{in}} - \underline{b} : \dot{\underline{\overset{\circ}{\alpha}}} - \kappa \bullet \dot{R} - \phi_{\mathrm{n}} \bullet \dot{D}_{\mathrm{n}} - \phi_{\mathrm{g}} \bullet \dot{D}_{\mathrm{g}} - \phi_{\mathrm{c}} \bullet \dot{D}_{\mathrm{c}} \geqslant 0. \tag{14}$$

in which, ϕ_{c}, is the generalized coalescence thermodynamic force conjugate (energy release rate) of the macroscale internal variable damage coalescence parameter, D_{c}, ϕ_{g}; ϕ_g is the generalized growth thermodynamic force conjugate (energy release rate) of the macroscale internal variable damage growth parameter, D_{g}; and ϕ_{n} is the generalized nucleation thermodynamic force conjugate (energy release rate) of the macroscale internal variable damage nucleation parameter, D_{n}. In essence, an increment of damage will have associated energy released per unit damage extension as new damaged area (or volume) is developed. The dissipation relation between the

thermodynamic conjugates including a coalescence term (and nucleation term for completeness) with a standard single void growth term.

One can certainly argue that separating void growth and coalescence may not be appropriate because of their intimate connection. But typical equations for single void growth have been formulated and have been used successfully in engineering practice thus encouraging their use. Hence, another term for coalescence would be needed in that context. Needleman and Tvergaard (1984) and Koplik and Needleman (1988) have proposed modifications to the Gurson (1977) model to account for coalescence. However, it was not until recently that Tvergaard and Needleman (1995, 1997) proposed a spatial gradient that represents effects of coalescence with a spatial characteristic size. If coalescence is modeled with spatial gradients such as the one proposed by Tvergaard and Needleman (1997), then one would need to include temperature effects based on the current study.

4. Conclusion

Displacement and force boundary conditions were applied to 6061T6 aluminum and 304L stainless steel with one and two voids at three different temperatures to show the effect of different states of plastic deformation and stress triaxialities acting upon the material. In general, the results confirm the need for including stress triaxiality and plastic deformation in a phenomenological void growth model (cf. Cocks and Ashby, 1980). However, these one void growth models typically do not capture multiple void effects. In this context, we propose a quantifiable definition of coalescence that is amenable to macroscale damage modeling. The major conclusions can be summarized as follows:

1. When multiple voids are present and within a critical intervoid ligament distance (ILD), the void growth rate is greater than a one void material with the same initial void volume.
2. Finite element calculations show that as temperature increases in the presence of multiple voids, the void growth rate increases. This occurs because plastic deformation greatly increases at higher temperatures although the stress triaxialities are almost equivalent.
3. No systematic trend exists for whether axisymmetric or planar 2D simulations give more void growth. In each case, the highest combination of the stress triaxiality and plastic deformation determines the extent of void growth.
4. Above a critical temperature, the effective plastic strain influences void growth more than stress triaxiality, but below a critical temperature, the stress triaxiality influences void growth more than the effective plastic strain.
5. The critical ILD for coalescence to enhance void growth depends on the material work hardening rate, temperature, orientation of holes with loading direction, and boundary conditions.
6. The work hardening rate plays a major role in the enhancement of void growth through coalescence. No major conclusion can be drawn about one material

experiencing more void growth than another at various temperatures because each material has a unique temperature dependence that changes the work hardening rate.
7. A transition from linear void growth to exponential void growth occurs as the stress triaxiality increases. The von Mises strain for this transition decreases with a multiple void configuration.

Acknowledgements

Appendix

Table A1
BCJ Material constants used for aluminum 6061T6 and 304L stainless steel[a]

	Aluminum 6061T6	304L stainless steel
E (GPa)	69.0	206.8
Poisson's ratio	0.33	0.30
Density (kg/m^3)	2700	7500
C1 (MPa)	0	5.309E+01
C2 (K)	0	9.453E+02
C3 (MPa)	3.768E+01	1.559E+02
C4 (K)	6.310E+02	1.105E+02
C5 (1/s)	1.000E+00	1.000E+00
C6 (K)	0	0
C7 (1/MPa)	3.262E+01	1.128E-03
C8 (K)	1.434E+03	−1796.200
C9 (MPa)	9.370E+02	4.820E+03
C10 (K)	1.230E+00	1.094E+01
C11 (s/MPa)	1.454E-03	2.385E-03
C12 (K)	2.521E+02	1.441E+03
C13 (1/MPa)	2.073E+05	1.674E-03
C14 (K)	6.394E+03	0
C15 (MPa)	6.777E+01	2.818E+03
C16 (K)	6.024E-02	4.622E+00
C17 (s/MPa)	3.913E-03	0
C18 (K)	2.468E+03	0
C19	1.700E-02	0
C20 (K)	7.700E+02	0

[a] Base units in MPa, m, s, K.

References

Al-Ostaz, A., Jasiuk, I., 1997. Crack initiation and propagation in materials with randomly distributed holes. Engin. Fract. Mech. 58 (5-6), 395.

Bammann, D.J., Chiesa, M.L., Horstemeyer, M.F., Weingarten, L.I., 1993. Failure in ductile materials using finite element methods. In: Jones, N., Weirzbicki, T. (Eds.), Structural Crashworthness and Failure. Elsevier Applied Science, p. 1.

Bammann, D.J., Chiesa, M.L., Johnson, G.C., 1996. Modeling large deformation and failure in manufacturing processes. In: Tatsumi, Wannabe, Kambe (Eds.), Theor. App. Mech., Elsevier Science, p. 259.

Bandstra, J.P., Goto, D.M., Koss, D.A., 1998. Ductile failure as a result of a void sheet instability: experiment and computational modeling. Matls. Sci. Engin. A., Structural Matls. Props. Micro. Proc. 249 (1), 46.

Benson, D.J., 1993. An analysis of void distribution effects on the dynamic growth and coalescence of voids in ductile metals. J. Mech. Phys. Solids 41 (8), 1285.

Benson, D.J., 1995. The effect of void cluster size on ductile fracture. Int. J. Plast. 11 (5), 571–582.

Briottet, L., Klocker, H., Montheillet, F., 1996. Damage in a viscoplastic material Part 1: cavity growth. Int. J. Plast. 12 (4), 481–505.

Brown, L.M., Embury, J.D., 1973. Proc. 3rd Int. Conf. on Strength of Metals and Alloys. Institute of Metals, London, p. 164.

Budiansky, B., Hutchinson, J.W., Slutsky, S., 1982. Void growth and collapse in viscous solids. In: Mechanics of Solids: The Rodney Hill 60th Anniversary Volume. Pergamon Press, Oxford, pp. 13–44.

Chan, K.S., 1988. The constitutive representation of high temperature creep damage. Int. J. Plast. 4, 355–370.

Cocks, A.C.F., Ashby, M.F., 1980. Intergranular fracture during power law creep under multixial stresses. J. Metal Science 14, 395.

Cocks, A.C.F., Ashby, M.F., 1982. On creep fracture by void growth. Progress in Materials Science 27, 189.

Cottrell, A.H., 1959. In: Averbach, B.L., Felbeck, D.R., Hahn, G.T., Thomas D.A. (Eds.), Fracture. Technology Press of MIT and John Wiley, New York.

Cuitino, A., Ortiz, M., 1992. A material independent method for extending stress update algorithms from small strain plasticity to finite strain plasticity with multiplicative kinematics. Engineering Computations 9, 437.

Eftis, J., Nemes, J.A., Randles, P.W., 1991. Viscoplastic analysis of plate-impact spallation. Int. J. Plast. 7, 15–39.

Faleskog, J., Shih, C.F., 1997. Micromechanics of coalescence — I. synergistic effects of elasticity, plastic yielding, and multi-size scale voids. J. Mech. Phys. Solids 45 (1), 21.

Garrison, W.M., Moody, N.R., 1987. Ductile fracture. J. Phys. Chem. Solids 48 (11), 1035–1074.

Geltmacher, A., Koss, D.A., Matic, P., Stout, M.G., 1996. A modeling study of the effect of stress state on void linking during ductile fracture. Acta Mater. 44 (6), 2201.

Geltmacher, A., Koss, D.A., Stout, M.G., Matic, P., 1998. Flow localizaion in sheet specimens with pairs of holes. Met. Trans. A, Phys. Metall. Matls. Sci. 29 (3), 775.

Gurson, A.L., 1977. Continuum theory of ductile rupture by void nucleation and growth: Part 1 — Yield criteria and flow rules for porous ductile media. ASME J. Engng. Mater. Techn. 99, 1–15.

Hibbitt, H.D., Karlsson, B.I., and Sorensen, E.P., 1998. ABAQUS-Standard, User Manual. Providence, RI.

Horstemeyer, M.F. and Ramaswamy, S., 2000. On factors affecting localization and void growth in ductile metals: a parametric study. Int. J. Damage Mech., in press.

Jun, S., 1991. Effect of stress triaxiality on micro-mechanisms of void coalescence and micro-fracture ductility of materials. Engineering Fracture Mechanics 39 (5), 799.

Koplik, J., Needleman, A., 1988. Void growth and coalescence in porous plastic solids. Int. J. Solids Structures 24 (8), 835.

Lee, Y.S., Dawson, P.R., 1993. Modeling ductile void growth in viscoplastic materials: void growth model. Mech. Of Matls. 15 (1), 21.

Lu, W.Y., Horstemeyer, M.F., Korellis, J.S., Grishibar, R.B., Mosher, D., 1998. High temperature sensitivity of notched AISI 304L stainless steel tests. Theoretical and Applied Fracture Mechanics 30, 139.

McClintock, F.A., 1968. A criterion for ductile fracture by growth of holes. J. Applied Mechanics 35, 363.

Moran, B., Ortiz, M., Shih, C.F., 1990. Formulation of implicit finite element methods for multiplicative finite deformation plasticity. Int. J. Numerical Methods in Engineering 29, 483.

Nagaki, S., Goya, M., Sowerby, R., 1993. The influence of void distribution on the yielding of an elastic-plastic porous solid. Int. J. Plasticity 9, 199–211.

Needleman, A., Tvergaard, V., 1984. An analysis of ductile rupture in notched bars. J. Mech. Phys. Solids 32, 461.

Nemes, J.A., Eftis, J., 1993. Constitutive modeling of the dynamic fracture of smooth tensile bars. Int. J. Plast. 9, 243–270.

Pardoen, T., Doghri, I., Delannay, F., 1998. Experimental and numerical comparison of void growth models and void coalescence criteria for the prediction of ductile fracture in copper bars. Acta Mater. 46 (2), 541.

Ramaswamy, S., Aravas, N., 1998. Finite element implementation of gradient plasticity models — Part 1: gradient dependent evolution equations. Computer Methods Applied Mech. Engin. 163 (1), 33.

Rice, J.R., Tracey, D.M., 1969. On the ductile enlargement of voids in triaxial stress fields. J. Mech. Phys. Solids 17, 201.

Thomson, C.I.A., Worswick, M.J., Pilkey, A.K., Lloyd, D.J., Burger, G., 1998. Modeling void nucleation and growth within periodic clusters of particles. Mech. Phys. Solids 47, 1.

Tonks, D.L., Thissell, W.R., Zurek, A.K., Hixson, R., 1997. Quantitative analysis of damage clustering in void linking for spallation modeling in tantalum. J. de Physique IV France 7 (C3), 841.

Tvergaard, V., Needleman, A., 1995. Effects of nonlocal damage in porous plastic solids. Int. J. Solids Structures 32 (8-9), 1063.

Tvergaard, V., Needleman, A., 1997. Nonlocal effects on localization in a void sheet. Int. J. Solids Structures 34 (18), 2221.

Worswick, M.J., Pick, R.J., 1995. Void growth and coalescence during high velocity impact. Mech. Of Matls. 19 (4), 239.

Worswick, M.J., Nahme, H., Fowler, J., 1994. Spall through void nucleation, growth, and coalescence. J. de Physique IV France 4 (C8), 707.

Zurek, A.K, Thissell, W.R., Tonks, D.L., Hixson, R., Addessio, F., 1997. Quantification of damage evolution for a micromechanical model of ductile fracture in spallation of tantalum. J. de Physique IV. France 7 (C3), 903.